

pubs.acs.org/JPCB Article

Connecting Non-Gaussian Water Density Fluctuations to the Lengthscale Dependent Crossover in Hydrophobic Hydration

Published as part of The Journal of Physical Chemistry virtual special issue "Pablo G. Debenedetti Festschrift". Imee Sinha, Steven M. Cramer, Henry S. Ashbaugh, and Shekhar Garde*



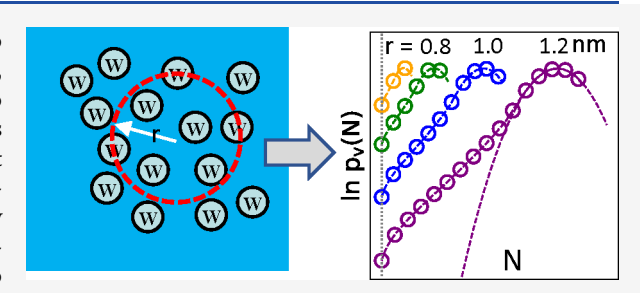
Cite This: J. Phys. Chem. B 2022, 126, 7604-7614



ACCESS

III Metrics & More

ABSTRACT: We connect density fluctuations in liquid water to lengthscale dependent crossover in hydrophobic hydration. Specifically, we employ indirect umbrella sampling (INDUS) simulations to characterize density fluctuations in observation volumes of various sizes and shapes in water and as a function of temperature and salt concentration. Consistent with previous observations, density fluctuations are Gaussian in small molecular scale volumes, but they display non-Gaussian "low-density fat tails" in larger volumes. These non-Gaussian tails are indicative of the proximity of water to its liquid to vapor phase transition and have implications on biomolecular



Article Recommendations

interactions and function. We show that the onset of non-Gaussian fluctuations in large volumes is accompanied by the formation of a cavity in the observation volume. We develop a model that uses the physics of cavity-water interface formation as a key ingredient and show that it captures the nature of non-Gaussian density fluctuations over a broad region in water and in salt solutions. We discuss the limitations of this model in the very low density region of the distribution. Our calculations provide new insights into the origins of non-Gaussian density fluctuations in water and their connections to lengthscale dependent crossover in hydrophobic hydration.

INTRODUCTION

Biomolecules contain a diversity of charged, polar, and hydrophobic groups, and their architecture and topology include many lengthscales ranging from that of a single amino acid to those of interfaces and assemblies of proteins. This assembly is mediated by water, and although the individual free energies of hydration and interactions of constituent groups can be large, their subtle balance leads to an overall thermodynamic stability of only a few tens of kT units.^{1–3} Calorimetry⁴⁻⁷ and other experiments⁸⁻¹¹ have highlighted the important role of hydrophobicity in driving biological assembly and in determining temperature, salt, and additive effects on their stability and interactions. 12,13

The seemingly simple process of dissolving a spherical nonpolar solute in water—hydrophobic hydration—displays a rather interesting dependence on solute size and thermodynamic conditions. 14,15 Although the hydration of both small and large hydrophobic solutes is unfavorable in water, their thermodynamics and mechanism of hydration are entirely different. The unfavorable hydration of small solutes is dominated by large negative entropy, whereas for large solutes it is the enthalpy that disfavors hydration. Small solutes can be readily accommodated into the molecular scale cavities that open up by spontaneous thermal fluctuations in liquid water. 16-18 To accommodate larger solutes, water must

nucleate an interface that is akin to a vapor-liquid interface, 14,19 which is somewhat entropically favorable but opposed by a large positive enthalpy. This crossover with increasing solute size, reflected in dewetting of the solutes and transition from entropy to enthalpy dominated hydration, is not sharp but occurs gradually for solutes of radii of about 1 nm or larger. 15,20

Connecting the thermodynamics of hydrophobic hydration to density fluctuations in water has been, perhaps, the most productive direction for inquiry over the past two decades.²¹⁻²⁴ The excess chemical potential of hydration of a hard particle solute, μ^{ex} , is related to the probability, $p_{\nu}(0)$, of observing 0 water molecules in a solute shaped observation volume ν , by

$$\mu^{ex} = -kT \ln(p_{\nu}(0)) \tag{1}$$

Received: July 14, 2022 Revised: September 7, 2022 Published: September 26, 2022





Hummer et al. expanded this view by considering $p_{\nu}(0)$ as one realization or event in the broader distribution, $p_{\nu}(N)$, describing the probability of observing N water molecules in v.²¹ Thus, quantifying or modeling the entire distribution, $p_{\nu}(N)$, provides a route to the chemical potential of a hydrophobic solute in water through $p_{\nu}(0)$. Hummer et al. showed that $p_{\nu}(N)$ s for small volumes are effectively Gaussian and can be easily modeled using its two moments, which can be calculated from water density and the water-water radial distribution function.²¹ Recently, Ashbaugh, Vats, and Garde demonstrated that Gaussian fluctuations away from the critical point can be accurately captured simply from knowledge of water's density and compressibility, eliminating the need to invoke the water structure for describing molecular-scale hydrophobic hydration.²⁵ Quantifying and understanding the nature of $p_{\nu}(N)$ is an important focus of the work presented here.

As v increases, $\langle N \rangle = \rho v$ also increases. That is, the mean of the distribution, $p_v(N)$, moves rightward, away from N=0. Therefore, calculation of μ^{ex} using eq 1, requires one to focus not on the nature of $p_v(N)$ near the mean but on the low-N tail of the distribution near $p_v(0)$. Using the Indirect Umbrella Sampling Method (INDUS), Patel et al, showed that with increasing v, the low-N tail of $p_v(N)$ displays increasingly non-Gaussian or fat-tail behavior. The values of $p_v(N)$ in this region are much higher than the corresponding Gaussian expectations, consistent with the formation of a vapor—liquid interface, and cross over to large lengthscale hydration.

Here, we systematically focus on the nature of density fluctuations in water and connect it to the crossover in hydrophobic hydration. We employ INDUS to quantify water density fluctuations, $p_{\nu}(N)$, in spherical volumes spanning a range from molecular to nanoscopic, and focus on the questions related to the emergence and nature of non-Gaussian behavior in the low-N tails of $p_{\nu}(N)$. For example, at what point does the transition from Gaussian to non-Gaussian fluctuations occur? Can simple physical models describe the non-Gaussian part of $p_{\nu}(N)$?

We also perform simulations over a range of temperatures and in the presence of salt to quantify how the thermodynamics of hydrophobic hydration and associated crossover depend on these thermodynamic parameters. In addition, how hydrophobic hydration depends on solute shape is of fundamental interest given the diversity of shapes encountered in biology. Therefore, we systematically study the hydration of solutes of different shapes (cubes, cuboids, cylinders, etc.). Our results add to the understanding of density fluctuations in water and their connections to the lengthscale dependent crossover in the hydration of hydrophobic solutes. 14,15,27,28

METHODS

We employed the Indirect Umbrella Sampling method²⁹ to quantify $p_{\nu}(N)$ in probe volumes of varying shapes ranging from molecular to nanoscopic in a systematic manner. We also studied temperature and salt dependence of hydration of selected solutes of different sizes. We provide the details below.

Isothermal–isobaric MD simulations of 11,225 SPC/E water molecules³⁰ were conducted in a cubic box of length \sim 7 nm using GROMACS³¹ in conjunction with INDUS sampling to quantify $p_{\nu}(N)$. A Nosé–Hoover thermostat^{32–34} and a Parinello–Rahman barostat³⁵ were used to maintain constant temperature and pressure with time constants of 0.5 and 1 ps, respectively. The particle mesh Ewald³⁶ method was

used to calculate electrostatics with a cutoff distance of 1 nm. A time step of 2 fs was used for all simulations. Configurations were saved every 2 ps.

Calculation of $p_v(N)$ **.** INDUS calculates $p_v(N)$ by performing umbrella sampling on the number of water molecules N in the probe volume, by biasing a coarse-grained variable, \tilde{N} , which is strongly correlated with N but varies continuously with particle coordinates. We refer the reader to Patel et al., which describes the challenges arising from umbrella sampling of point particles (water centers) in a volume and the coarse-graining employed by INDUS to resolve this. The number of INDUS windows required to sample $p_v(N)$ ranged from 5 for small volumes to as large as 50 (for the 1.8 nm sphere). The INDUS coarse-graining parameters of $\sigma = 0.01$ and $\alpha = 0.02$ were used in all simulations. Each simulation window was equilibrated for 1 ns followed by a production run of 2 ns.

Size and Shape Dependence. To characterize the size-dependent hydration thermodynamics, we studied spherical probe volumes of radii 0.2, 0.4, 0.6, 0.8, 1.0, 1.2, and 1.8 nm (see Figure 1). We also studied cubic probe volumes having

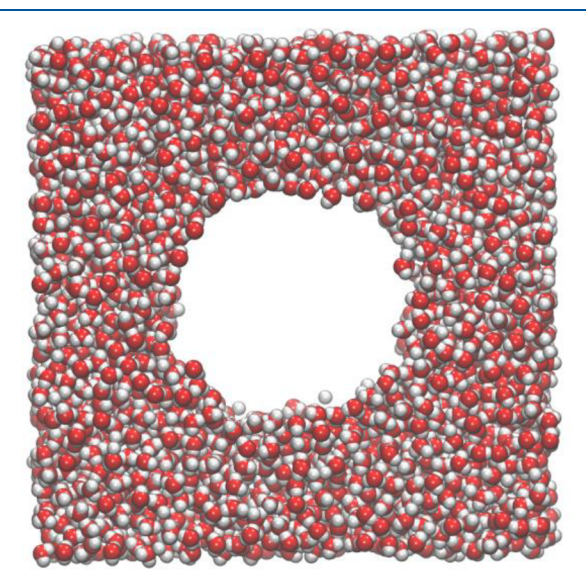


Figure 1. A large cavity in water. A snapshot from a molecular dynamics simulation of water performed using indirect umbrella sampling illustrates the nature of a large spherical cavity in water (radius \sim 1.8 nm) in a \sim 7 nm cubic box. For clarity, only the water molecules in a 1 nm thick perpendicular cross-section are shown in the spacefill representation [oxygen (red), hydrogen (white)] rendered using VMD.³⁷

the same corresponding volumes as each of these spherical volumes. Side lengths of these cubic volumes ranged from about 0.3 to 2.9 nm. To quantify shape dependence of $p_{\nu}(N)$, we studied a sphere, cube, cuboid, and cylinder, all having the same volume, equal to that of sphere of radius 0.6 nm.

Temperature and Salt Dependence. To study the thermodynamics of hydrophobic hydration, we performed simulations at three different temperatures 275, 300, and 325 K for spherical probes of radii 0.2, 0.6, and 1.2 nm in bulk water. We also performed INDUS calculations for spherical probes of radii 0.6 and 1.2 nm in 1 and 2 M NaCl salt solutions. We represented sodium and chloride ions as spherical Lennard–Jones solutes with a unit electronic charge placed at their centers. ³⁸

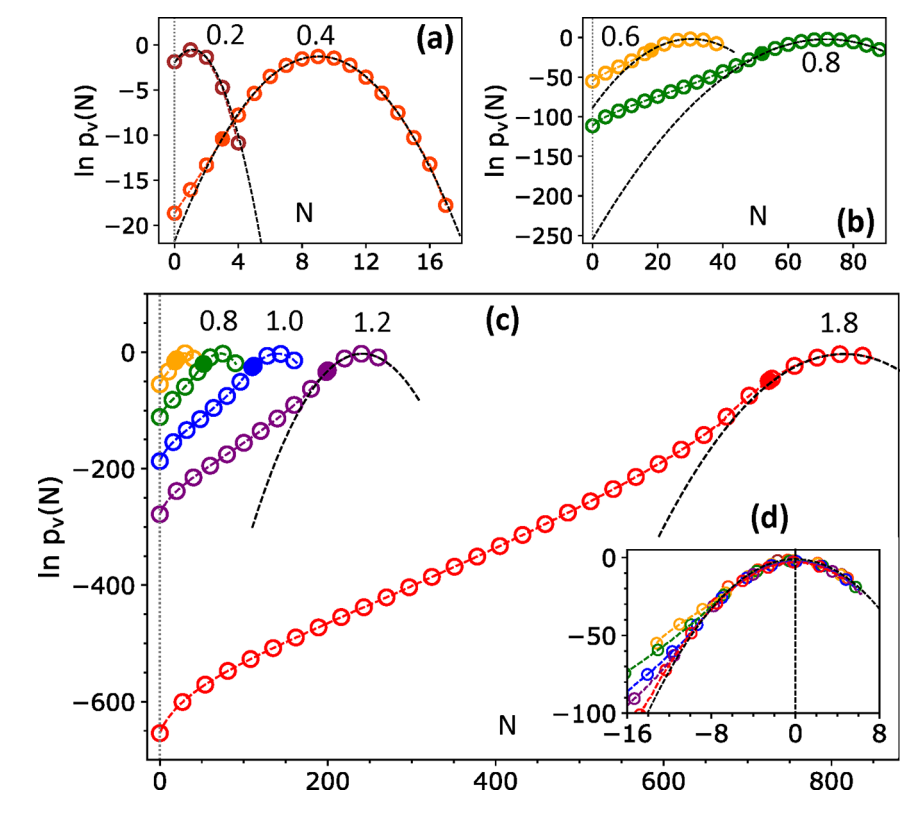


Figure 2. Water density fluctuations in spherical observation volumes: Probability, $p_{\nu}(N)$, of observing N water molecules in spherical volumes of radii 0.2 to 1.8 nm are shown in panels a—c on a log—linear scale. Open circles show $p_{\nu}(N)$ s obtained from INDUS simulations, whereas dashed black lines show the Gaussian expectation using the same mean and the variance. The filled circles show the point obtained from theoretical arguments (see text), indicating the number, N^* , below which fluctuations become distinctly non-Gaussian. Panel d shows density fluctuations on a normalized x-axis, $\left(\frac{(N-\langle N \rangle)}{\sigma}\right)$. Error bars on these plots are smaller than the size of symbols used.

RESULTS AND DISCUSSION

Water Density Fluctuations in Spherical Volumes of **Increasing Radius.** Figure 2 shows water density fluctuations, $p_{\nu}(N)$, in spherical observation volumes of radii ranging from 0.2 to 1.8 nm. For reference, Gaussian density fluctuations (with the same mean and the variance) are shown with dashed lines, which are parabolic on a log scale. For the smallest sphere (r = 0.2 nm), $p_v(N)$ is almost exactly Gaussian over the entire range of N (Figure 2a). Consistent with Hummer et al.²¹ and many other previous calculations, $^{22,23,39}p_{\nu}(N)$ for a sphere with radius of 0.4 nm is also mostly Gaussian, except near the low-N tail (specifically for N = 0 and 1). If water molecules were uncorrelated with each other, like ideal gas particles, one would expect a Poisson distribution for $p_{\nu}(N)$, which in the large volume limit becomes Gaussian. However, it is the correlations that make water interesting and special, and their impact is evident in the non-Gaussian density fluctuations, reflected in the low-N fat tails of $p_{\nu}(N)$ for larger observation volumes (Figures 2b and 2c). Figure 2d shows $p_{\nu}(N)$ for all volumes plotted using a normalized horizontal axis. As expected, $p_{\nu}(N)$ is roughly Gaussian near the mean for all volumes, but becomes non-Gaussian as N is reduced by more than $\sim 4\sigma$. We note that error bars on the energetic quantities (e.g., $\ln p_{\nu}(N)$) reported in Figure 2 as well as other figures in this manuscript (except Figure 7b) are on the order of few kJ/ mol, usually comparable to or smaller than the size of symbols used, and are therefore not shown explicitly.

As described by Patel et al.,⁴⁰ the transition to non-Gaussian density fluctuations and the associated low-N fat tail in $p_{\nu}(N)$

suggest that water under ambient conditions is near its liquid to vapor phase transition. As the overall density in the observation volume is reduced sufficiently, a cavity is nucleated within the volume with its interface akin to that of the vapor—liquid interface of water. The free energy of creating such a cavity is given by $4\pi r^2 \gamma$, where γ is the surface tension. This value of free energy is lower than the corresponding value obtained using the Gaussian route, thus providing an alternate and less costly path to dewetting the volume. This is really the essence of the Gaussian to non-Gaussian transition in density fluctuations observed in Figure 2.

At what N does the non-Gaussian behavior become evident? Can we predict $p_{\nu}(N)$ over the non-Gaussian range? Below we present an approximate analysis that addresses these two questions.

For density fluctuations near the mean, we define the free energy along the coordinate N by $\beta G_{Gauss}(N) = -\ln p_{\nu}(N)$. Thus,

$$\beta G_{Gauss}(N) = \frac{(N - \langle N \rangle)^2}{2\sigma^2} + \frac{1}{2}\ln(2\pi\sigma^2)$$
 (2)

Depleting N sufficiently nucleates a cavity that is smaller than the observation volume and may fluctuate in shape, as well as move about within the volume. Assuming that the cavity is spherical, its radius is given by $r = \left[\frac{\langle N \rangle - N}{4\pi\rho/3}\right]^{1/3}$, with the corresponding free energy given by

$$\beta G_{non-Gauss}(N) = 4\pi \left[\frac{\langle N \rangle - N}{4\pi \rho/3} \right]^{2/3} \beta \gamma + C$$
(3)

where *C* is a constant, ρ is the density of water, and $-\ln p_{\nu}(N < \langle N \rangle) = \beta G_{non-Gauss}(N)$ represents the non-Gaussian part of density fluctuations $p_{\nu}(N)$.

The functions $G(N)=-kT\ln(p_{\nu}(N))$ in the Gaussian or non-Gaussian parts of the density fluctuations are effectively the potentials of mean force along the N coordinate. Equating their slopes (i.e., the mean force $-\frac{\partial G}{\partial N}$ along N) provides the transition point N^* as

$$N^* = \langle N \rangle - \left(\frac{32\pi}{3}\right)^{1/4} \left(\frac{\beta \gamma}{\rho^{2/3}}\right)^{3/4} \sigma^{3/2}$$
 (4)

Equating the value of $G(N^*)$ for Gaussian and non-Gaussian PMFs provides the value of constant C in eq 3.

Similar to information theory based modeling of hydrophobicity, 21 eq 2 only needs information about water density, ρ , and variance, σ^2 . The variance can be obtained by integration of water—water radial distribution function available from experiments. Equation 3 requires information about surface tension and density of water, which are available experimentally. Note that in developing eq 3, we use a constant value for surface tension, and also ignore the entropic contributions arising from cavity movement inside the observation volume.

Figure 3a shows slopes, $-\beta \partial G/\partial N$, obtained using the above approach for a spherical observation volume with radius of 1.8 nm. Intersection of these curves gives N^* (marked in gray), also shown in Figure 3b for several probe volumes as well as

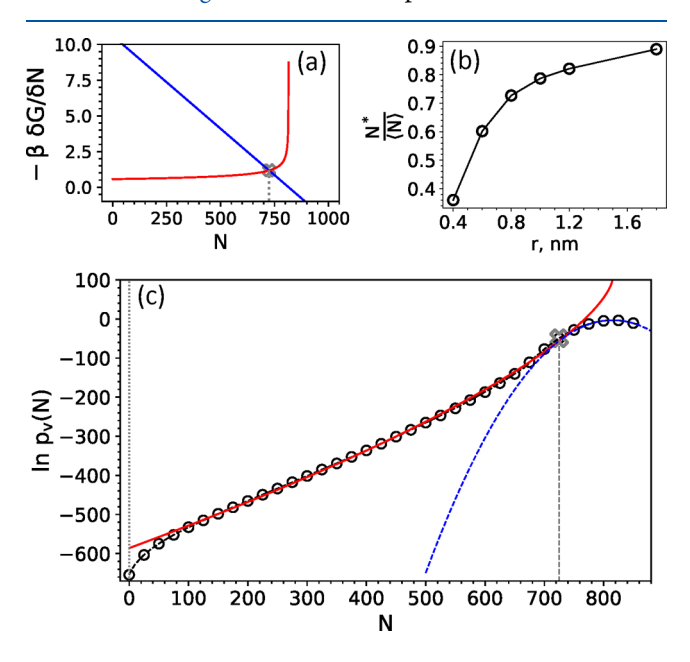


Figure 3. (a) Slopes $-\beta\partial G/\partial N$ of G_{Gauss} (blue) and $G_{non-Gauss}$ (red) intersect at $N^*=725$ for a probe of radius 1.8 nm. We used the value of surface tension to be 41.9 kJ/mol/nm², which is equal to γ in the large lengthscale limit. (b) Variation of $\frac{N^*}{\langle N \rangle}$ as a function of radius of the probe volume. (c) Density fluctuations, $p_{\nu}(N)$, for a spherical cavity of radius 1.8 nm: data from INDUS (symbols), Gaussian expectation (dashed blue line), theoretical prediction using eq 3 (solid red line).

marked on the panels in Figure 2. Indeed, N^* marks the beginning of the non-Gaussian tail quite well, which is remarkable given the simplicity of the assumptions that go into its derivation. For small cavities, $N^*/\langle N \rangle$ is about 0.35, and increases with increasing ν as shown in Figure 3b. Thus, for small ν , $p_{\nu}(N)$ is Gaussian over a larger fraction of the curve, whereas with increasing ν , the range, $N > N^*$, over which $p_{\nu}(N)$ is Gaussian diminishes asymptotically.

Finally, Figure 3c shows the prediction of non-Gaussian part of the $p_{\nu}(N)$ for the largest spherical observation volume of radius 1.8 nm. Over the range from N^* (equal to 725, marked in gray), down to about N=100, there is a very good agreement between the predictions of eq 3 and the data obtained from INDUS simulations. For values of N lower than 100, there is a clear downturn in $p_{\nu}(N)$. This observation is consistent with the fact that the free energy landscape along N is not wholly convex over the entire range of N.

Prediction of the exact nature of $p_{\nu}(N)$ in the very low-*N* tail approaching N = 0 is tricky for it partly captures the difference between free energies of hydration of a soft and a hard cavity. That is, it roughly captures the difference between forming a 1.8 nm sized bubble with a soft vapor-liquid interface and forming a completely empty cavity (N = 0) that can accommodate a hard-sphere solute of radius 1.8 nm inside it. As N goes from its average value of \sim 825 down to 100, a large cavity that is about the size of the observation volume is formed. To remove the remaining 100 or so water molecules from this cavity requires that all the soft tails of water density (i.e., surface capillary fluctuations 42 that intrude into the observation volume) are ironed out or pushed out of the volume. A theoretical treatment of this feature is beyond the scope of the present manuscript, but it would be a useful direction to pursue in the future. Nevertheless, that a simple non-Gaussian prediction does such a remarkable job over a broad range of N from N^* (725) down to 100 is noteworthy.

As stated above, the onset of non-Gaussian behavior in $p_{\nu}(N)$ is associated with the formation of a stable cavity in the observation volume, which grows in size with further decrease in N. Interestingly, the transition from Gaussian to non-Gaussian branch is also visible in the dynamics of water numbers in the observation volume in different windows of INDUS simulations.

Figure 4a focuses on $p_{\nu}(N)$ for 1.8 nm radius sphere in the region of Gaussian to non-Gaussian transition. N^* obtained from eq 4 is shown by the filled gray circle. Parts c-e of Figure 4 show the dynamics of water molecules, N(t), over a 4 ns piece of trajectory obtained from INDUS umbrellas placed to the right of N^* (on the Gaussian branch, Figure 4c), in the vicinity but to the left of N^* (in the transition region, Figure 4d), and to the further left of N^* squarely in the non-Gaussian region (Figure 4e). The behavior of N, i.e., its distribution and dynamics, in a given umbrella window are determined by the combination of the quadratic umbrella potential and the system Hamiltonian that governs the underlying PMF, -kT ln $p_{\nu}(N)$.

In umbrella windows in the Gaussian (Figure 4c) and fully non-Gaussian regions (Figure 4e), the fluctuations of N are well-defined and within ± 15 of the average, consistent with local thermal fluctuations in a quadratic well. In the transition region, however, the combination of umbrella potential and the underlying Hamiltonian leads to a wider underlying basin that allows excursions of N(t) as far away as ± 30 from the average in that window (Figure 4d). The enhanced fluctuations of N(t) in

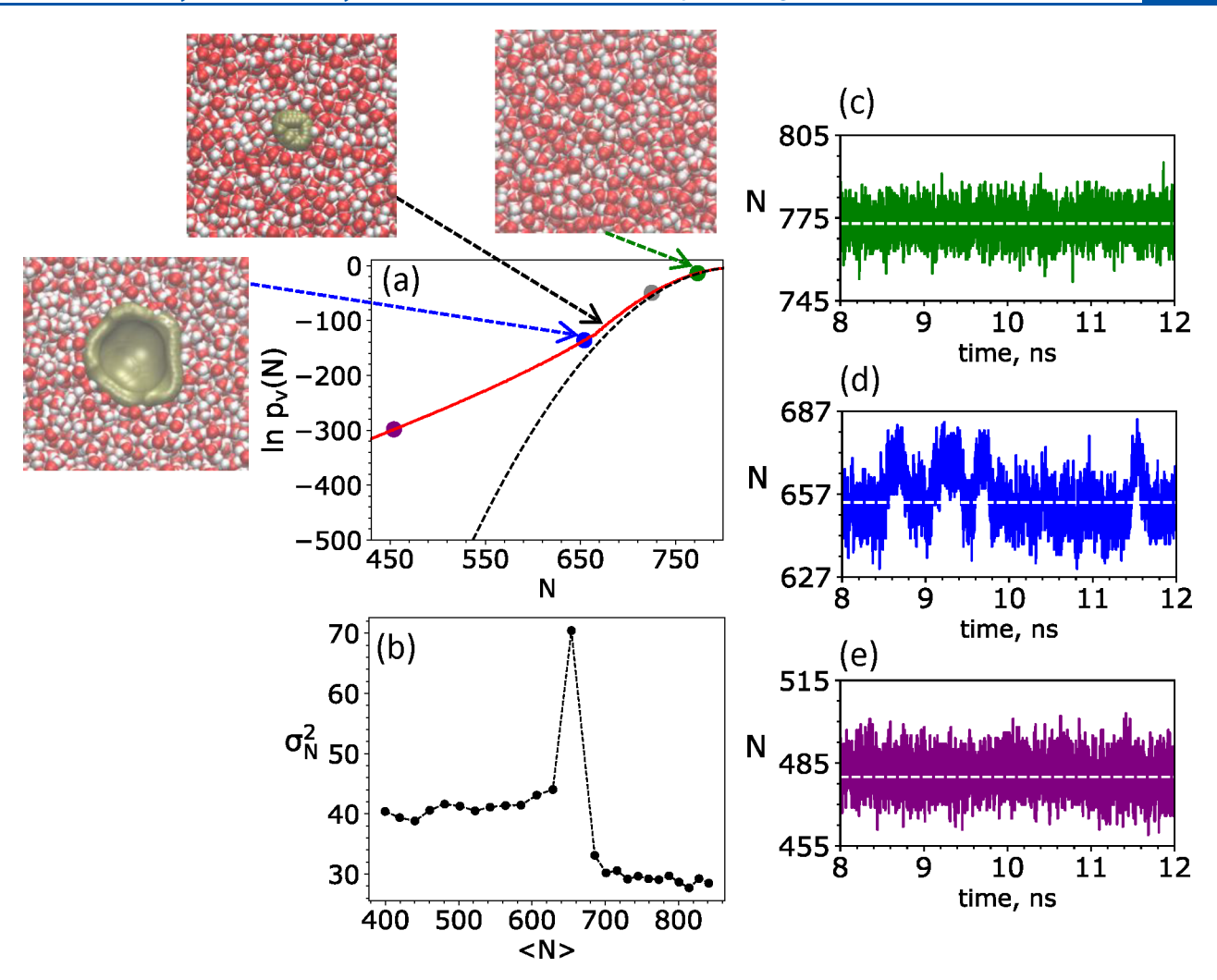


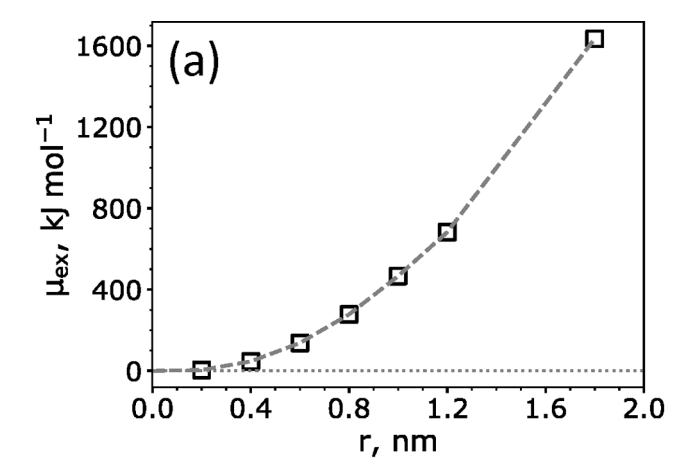
Figure 4. (a) $p_v(N)$ for a spherical volume of radius 1.8 nm in the Gaussian to non-Gaussian transition region. The point of transition, $N^* = 725$ is shown in filled gray circle. (c-e) N vs t dynamics observed in three INDUS windows placed relative to N^* as described in the text. The centers of umbrella potentials, \tilde{N}_u , for windows in panels c-e are at 754, 614, and 454, respectively. The corresponding average values of N in these three windows are shown by dashed white lines in the panels and also by filled colored circles in panel a. Snapshots of an instantaneous cavity observed in INDUS simulations are also shown, using the Willard-Chandler cavity-water interface 43 colored in gold. (b) Variance, σ_N^2 , as a function of $\langle N \rangle$, obtained from different umbrella windows, which displays a peak in the transition region.

INDUS windows in the transition region are also evident in the variation of σ_N^2 vs $\langle N \rangle$ shown in Figure 4b. Xi et al. ⁴¹ in their work focused on sparse sampling of water density fluctuations provide an explanation of the peak in σ_N^2 observed in Figure 4b. They show that σ_N^2 in a given INDUS window is related to the second derivative of the free energy with respect to N: $1/\beta\sigma_N^2=\frac{\partial^2 G}{\partial N^2}+\kappa$, where κ is the spring constant used in the harmonic biasing potential in INDUS. Thus, the peak in σ_N^2 in Figure 4b corresponds to an inflection point in the underlying G(N) curve, indicating transition from Gaussian to non-Gaussian fluctuations.

Lengthscale Dependence of the Free Energy of Hydration. Figure 5a shows the free energy of creating a spherical cavity of radius ranging from 0.2 to 1.8 nm obtained using eq 1 and INDUS simulations. The size dependence of cavity formation free energy has been studied by many researchers in the past, ^{15,20,21,44–46} and the key features of the data in both parts a and b of Figure 5 are well understood. Under ambient conditions, Gaussian density fluctuations in water lead to spontaneous formation of small molecular scale

cavities. The free energy of hydration for such small cavities is roughly proportional to cavity volume. Creation of larger cavities (~1 nm or larger), however, requires formation of a vapor-liquid like interface. The free energy of creating such cavities scales with the surface area of the cavity. This transition from small to large lengthscale hydration is clear in Figure 5b, which shows the lengthscale dependence of the free energy of cavity hydration per unit surface area. For small cavities, Gaussian predictions (red dashed line) work well, but with an increasing cavity size, the free energy per unit surface area approaches the macroscopic surface tension, γ_{∞} . The γ_{∞} value of 41.9 kJ/mol/nm² is in good agreement with that obtained by Vega et al.⁴⁷ (38.3 kJ/mol/nm²) and also within 2% of the experimental value of the water surface tension (42.88 kJ/mol/nm²).⁴⁷ The Tolman equation, which describes the leading order curvature dependence of the surface tension, fits the data for larger cavities well.

Shape-Dependent Hydrophobicity. In addition to size, the free energy of hydration of a hydrophobic solute also depends on its shape. 40,48,49 Sedlmeier and Netz have presented an excellent analysis of the comparison of hydration



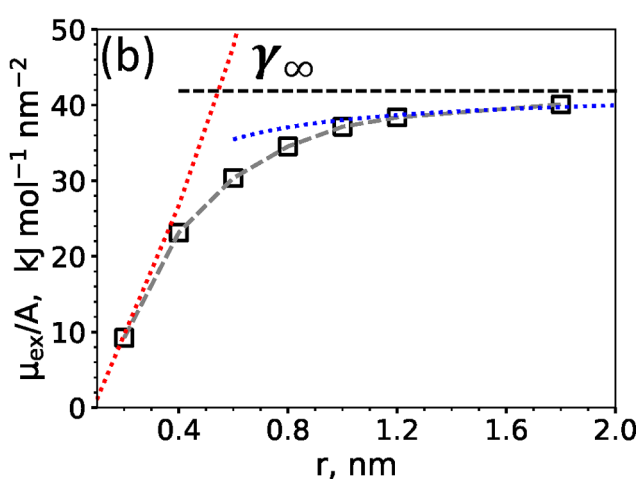


Figure 5. Lengthscale dependent free energy of hydration of spherical solutes. (a) Free energy, μ^{ex} , of creating spherical cavities of radii 0.2 to 1.8 nm in water obtained using INDUS (symbols). (b) The quantity $\mu^{ex}/4\pi r^2$ shows crossover in hydration from small to large spherical solutes. Gaussian prediction of $\mu^{ex}/4\pi r^2$ (dotted red line) and a fit to the Tolman equation, $\gamma = \gamma_{\infty}(1-2\delta/R)$, with $\gamma_{\infty} = 41.9 \text{ kJ/mol/nm}^2$ and $\delta = 0.046$ nm are shown (dotted blue line). γ_{∞} is marked with a dashed black line.

of spheres and cylinders of various sizes and their crossover from small to large lengthscales. 46 Both the size dependence and shape dependence of hydration are evident in the collapse of a hydrophobic polymer in water, where the hydration of a larger globular collapsed state is more favorable than the sum of the hydration free energy of many small monomers representing the unfolded state. 14,50,51

To quantify the shape dependence of hydrophobicity, we studied the hydration of four different shapes—a sphere, a cube, a cuboid with width 0.3 nm, and a cylinder with radius 0.3 nm—all having the same volume as that of a sphere of radius 0.6 nm (Figure 6a). We employed INDUS to calculate $p_v(N)$ in observation volumes of these four shapes.

The sphere and the cube have one characteristic length corresponding to the radius (0.6 nm) or the side length (0.96 nm), whereas the cuboid and the cylinder have two relevant lengths. As shown in Figure 6a, one of the characteristic lengths for the cuboid and cylinder is small, comparable to that of the size of a water molecule. Thus, water molecules in the liquid can either interact across such small lengths or accommodate such objects by forming a hydrogen-bonding network around them. The nature of density fluctuations

shown in Figure 6b is influenced by the relevant lengthscale of the objects studied. $p_{\nu}(N)$ for the thin cuboid, and the cylinder is closer to the Gaussian expectation, whereas the cube and sphere display a pronounced non-Gaussian tail, indicative of interface formation and large lengthscale hydration. As expected from results in Figure 2, creation of a vapor—liquid like interface provides an alternate lower free energy path to hydrate an object. Thus, it is more costly to hydrate a thin cuboid or a cylinder than a cube or a sphere of the same volume.

Figure 6c shows the variation of the effective surface tension of solute-water interface, μ^{ex}/A , as a function of curvature (defined as A/V). The trend is consistent with that observed in Figure 5b. Of course, for the cuboid and the cylinder, the apparent surface tension is smaller, but the overall surface area is large, making their hydration costlier than that for the cube or the sphere.

Figure 6d shows μ^{ex} for spheres and cubes having the same volume, corresponding to spheres with radii ranging from 0.2 to 1.8 nm (same as in Figure 5a). For convenience, the μ^{ex} values for cubes are shown along with the spheres at the same horizontal location (r). As expected, for the same volume, it is more favorable to hydrate a sphere than a cube. With increasing size, both the spheres and cubes display the expected lengthscale crossover (Figure 6e). For the sizes of cubes studied here, the eight corners (near which water molecules can interact around or across them) still influence the effective surface tension, lowering it relative to spherical shapes of the same volume. However, in the large lengthscale limit, we expect both to approach γ_{∞} .

The shape and size dependence of hydrophobic hydration discussed above has implications on self-assembly. For example, aggregation of n smaller spheres into a larger spherical globule is expected based on the lengthscale dependence shown in Figure 5. However, based on Figure 6, we expect that driving forces will be different for aggregation of cubes with other cubes, of cylinders with other cylinders, or of plates with other plates. One expects cylinders or plates to align parallel to each other. Assembly of other shapes, such as cones (not studied here), or mixtures of above shapes will provide an even richer landscape for future studies. Such assembly phenomena and their mechanisms (e.g., in what configurations do objects approach each other? What is the reaction coordinate for their assembly?) would be interesting to study in the future, leading possibly to an expansive design perspective for self-assembly of objects with complex shapes.

The Thermodynamic Crossover. There are three crossovers ^{15,19,52–54} in lengthscale dependent hydrophobic hydration. One is shown in Figure 5b. The second one, the structural crossover, refers to the gradual dewetting of the surface of a hydrophobic solute with increasing solute size. The third, shown in Figure 7, focuses on thermodynamic signatures of hydration. The hydration of small solutes is dominated by a large negative entropy of hydration, whereas for large solutes, it is governed by unfavorable enthalpy of interface formation. Results shown in Figure 7 are consistent with this picture.

Figure 7a shows the temperature dependence of μ^{ex}/A along the crossover curve. While the changes are subtle, we observe that the free energy of hydration of a sphere of radius 0.2 nm increases with increasing temperature, whereas the reverse is true for the sphere of radius 1.2 nm. The variation of μ^{ex}/A with temperature is clearer in Figure 7b, where the slope changes from positive for the small solute to negative for the

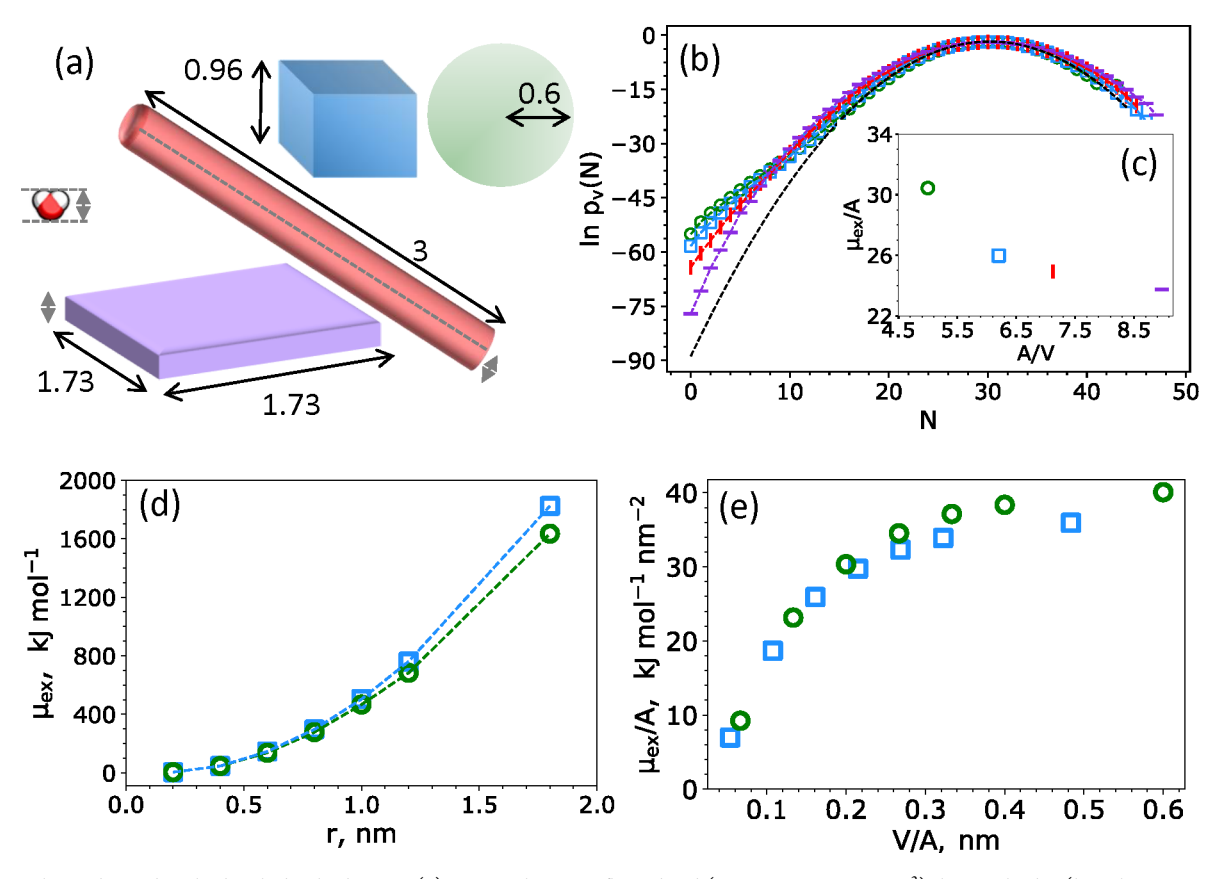


Figure 6. Shape-dependent hydrophobic hydration. (a) Cavity shapes: a flat cuboid $(1.73 \times 1.73 \times 0.3 \text{ nm}^3)$, long cylinder (length 3 nm, radius 0.3 nm), cube (side 0.96 nm), and a sphere (radius 0.6 nm). (b) $p_{\nu}(N)$ for cavities of four different shapes having the same volume as that of the 0.6 nm radius sphere shown in panel a. The symbols in panel b use the same colors and shapes as the objects in panel a. (c) Free energy of cavity formation per unit area as a function of curvature (surface area divided by volume). (d) Variation of free energy of cavity formation of cubic and spherical cavities of the same total volumes, plotted as a function of radius of spherical cavities. (e) Free energy of cavity formation per unit area for cubic and spherical cavities as a function of their inverse curvature.

larger one, consistent with the temperature dependence of surface tension of water.

We resolve μ^{ex} into its entropic and enthalpic contributions for the three solutes, as shown in Figure 7c–e. Again, as expected, the free energy of hydration for the smallest sphere is dominated by negative entropy, whereas for the large sphere, where the hydration is dominated by the physics of interface formation, the enthalpy of hydration is large and positive, unfavorable, and the entropy is actually slightly favorable. These results are consistent with previous calculations by Rajamani et al. 15 and others. 25,53,55,56 As discussed by Rajamani et al., the different temperature dependences of the free energy of hydration of small and large solutes provides a handle to manipulate the crossover length. For example, at higher temperatures, a combination of lower γ_{∞} and higher μ^{ex}/A for smaller solutes, leads to reduction of the crossover length.

Salt Effects on Hydrophobic Hydration. Unlike temperature, which affects the hydration of small and large solutes differently, adding salt to the solution has a qualitatively similar effect on the hydration of small and large solutes. Typical salt ions are well hydrated in water, and they preferentially exclude themselves from the vicinity of hydrophobic solutes. Such depletion increases the effective interfacial tension of the solute—water interface and makes solute hydration unfavorable. ^{57–61}

Figure 8a shows the effect of adding 1 and 2 M NaCl to solution on μ^{ex}/A of two spherical solutes of radii 0.6 and 1.2 nm. Increasing salt concentration increases the free energy of hydration monotonically as shown in parts a and b of Figure 8. The increase in effective surface tension of 1.2 nm sphere with addition of salt is similar to that observed for the salt dependence of the liquid—vapor surface tension of water. Setchenow's coefficients, obtained from fitting the data in Figure 8b, are 0.81 and 3.86 L/mol, respectively for the two solutes, which are consistent with those inferred for spherical solutes previously. 61,62

Parts c—e of Figures 8 show $p_{\nu}(N)$ distributions for 1.2 nm sphere obtained from INDUS simulations in pure water and in 1 and 2 M salt solutions, respectively. The figure focuses on the Gaussian to non-Gaussian transition region. It is noteworthy that fits using eq 3 with surface tensions of 43 kJ/mol/nm² (0 M), 45 kJ/mol/nm² (1 M), and 46 kJ/mol/nm² (2 M) for three solutions represent the nature of $p_{\nu}(N)$ curves reasonably well, again consistent with a salt-induced increase in the surface tension of water. Although we have only studied the common salt, NaCl, it would be of interest in the future to study systematically the effects of various kosmotropic and chaotropic salts on the hydration of hydrophobic solutes of various sizes.

We note that alternative approaches exist for predicting cavity formation free energies in liquids. For example, Dor Ben-Amotz proposed a cavity equation of state to obtain free

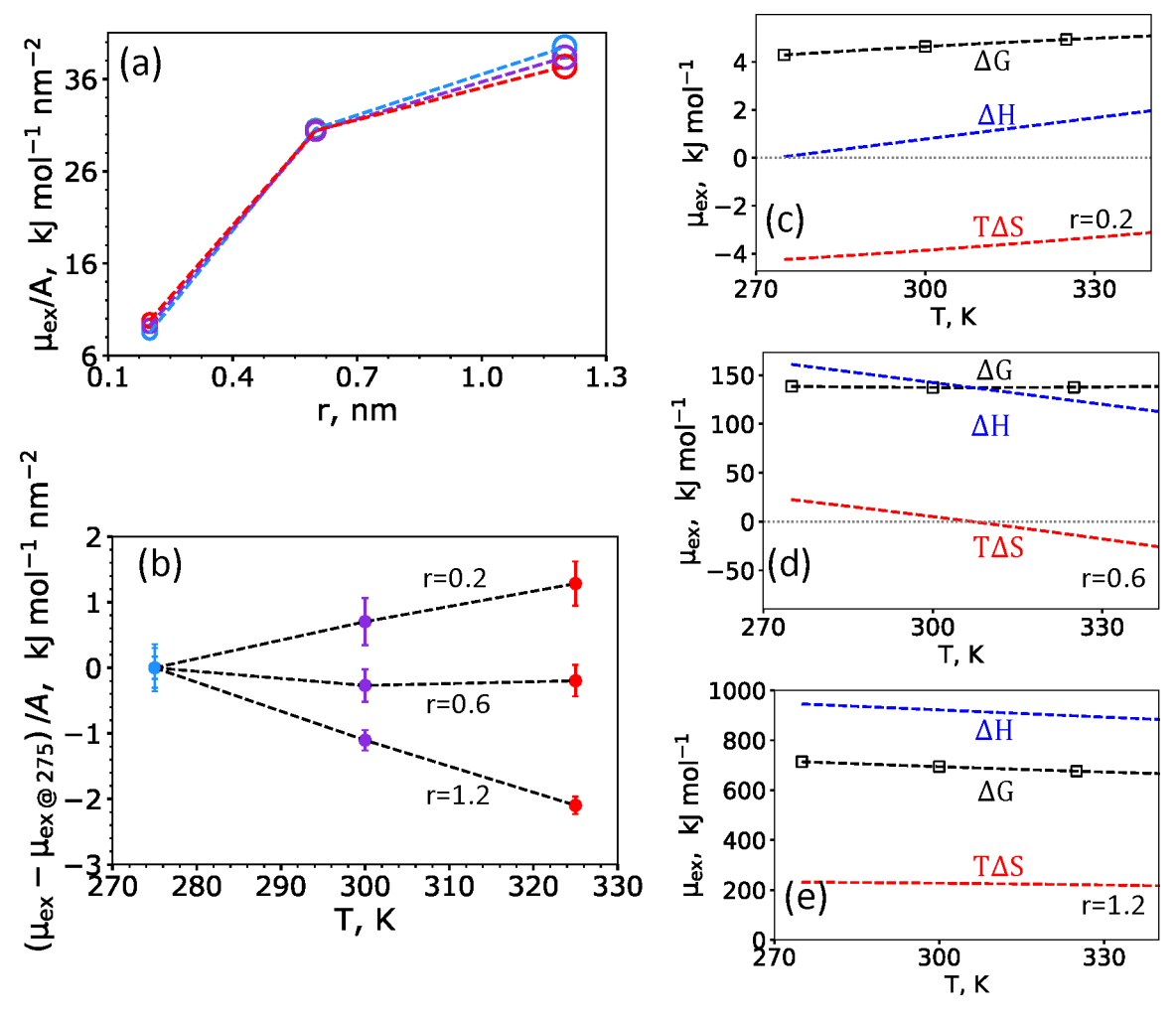


Figure 7. (a) μ^{ex}/A for spherical cavities of radii 0.2, 0.6, and 1.2 nm at 275 (blue), 300 (violet), and 325 K (red). (b) $[\mu^{ex}(T) - \mu^{ex}(275)]/A$ as a function of temperature for the three cavity sizes. Entropy and enthalpy contributions to the free energy of hydration of spherical cavities of radius 0.2 (c), 0.6 (d), and 1.2 nm (e), respectively. Dashed lines are obtained from fits to simulation data (squares).

energy of cavity formation in hard-sphere or hard-body fluids for cavities with spherical as well as anisotropic shapes. 63-65 We find that the cavity equation of state works well for predicting free energies (if not the enthalpy and entropy contributions) for hydration of spherical cavities in water. Our thermodynamic data on the hydration of different cavity shapes and over a range of temperatures and salt concentrations presented here could be used in the future to test and refine those theories. Finally, given the interest in various water models, it may be useful in the future to perform calculations similar to ours for a range of water models.

CONCLUSIONS

Interest in the lengthscale dependence of hydrophobic hydration traces its roots to the development of scaled particle theory by Reiss⁶⁶ and the seminal work by Stillinger. ¹⁹ Over the next decades, increasing computing power coupled with development of enhanced sampling algorithms for molecular simulations has made it possible to answer many of the fundamental questions in a systematic manner. We focused on quantifying density fluctuations, $p_{\nu}(N)$, in solute-shaped observation volumes in water over a range of solute sizes, shapes, and solution conditions. That $p_{\nu}(N)$ s are Gaussian in small volumes in water has been known since 1996.²¹ The

development of INDUS²⁹ allowed sampling of fluctuations in much larger volumes, and highlighted the emergence of low-N non-Gaussian tails in $p_{\nu}(N)$, consistent with the proximity of water under ambient conditions to its liquid—vapor phase transition. Such non-Gaussian fluctuations are known, ^{22,23} and their relevance to biological function has also been studied. ⁴⁰ Quantitative questions about the emergence of and the nature of the non-Gaussian behavior have, however, not been answered to date. For example, at what point does the transition from Gaussian to non-Gaussian fluctuations occur? And can simple physical models describe the non-Gaussian part of $p_{\nu}(N)$?

We showed that the emergence of non-Gaussian behavior is accompanied by creation of a stable cavity in the volume with a vapor—liquid like interface. The physics of interface formation can be used to model non-Gaussian density fluctuations over a broad region, not only in bulk water but also in salt solutions. That a simple surface tension based model can predict the non-Gaussian part of $p_{\nu}(N)$ over a broad range is noteworthy. Yet, our approach is incomplete because the near-zero tail of $p_{\nu}(N)$ remains unresolved. The challenges in modeling $p_{\nu}(N)$ or the PMF, $-kT \ln p_{\nu}(N)$ over the entire range of N arise from the fact that the PMF displays wholly nonconvex behavior, indicative of a double well free energy landscape under

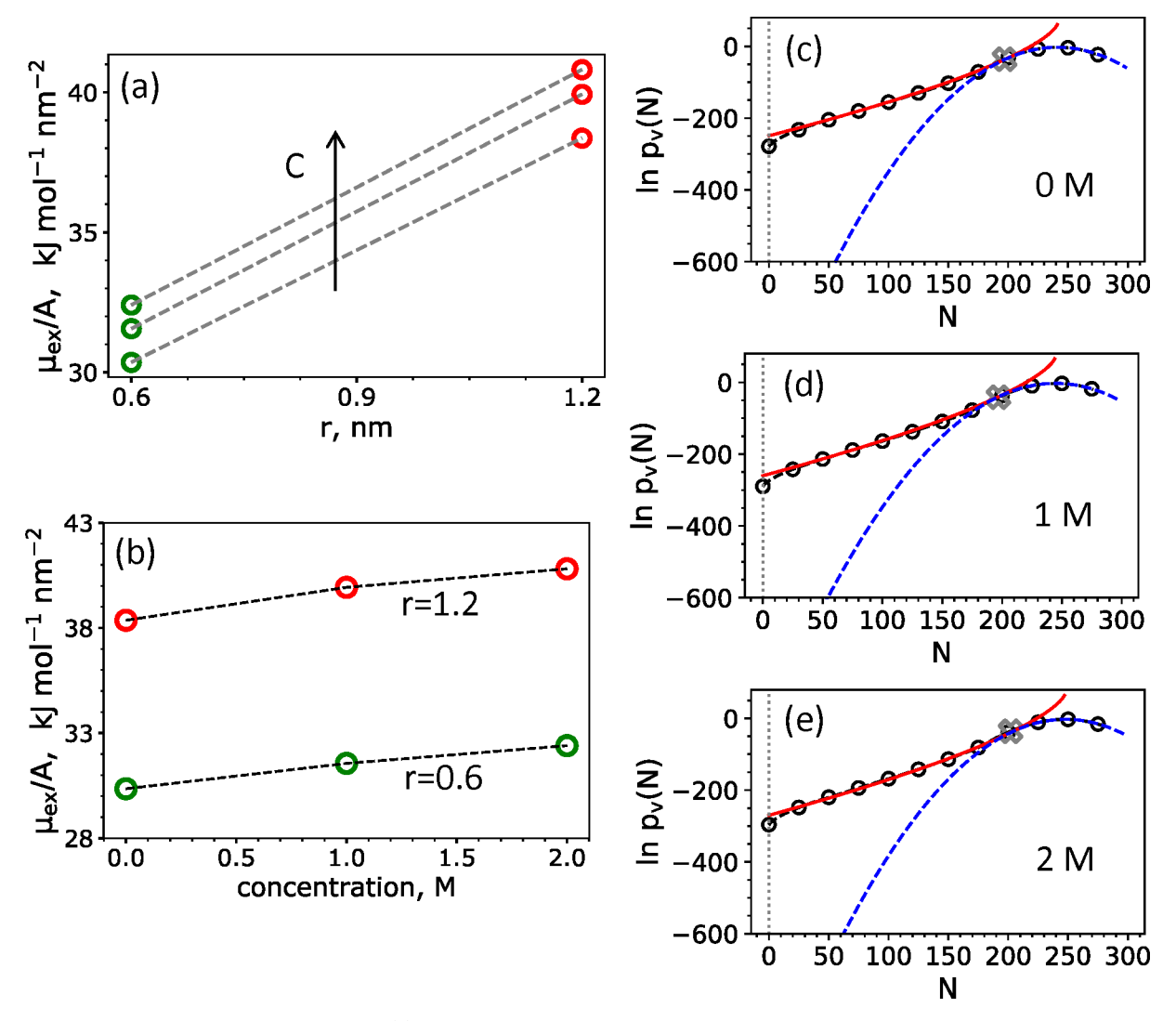


Figure 8. Salt effects on hydrophobic hydration. (a) μ^{ex}/A for spherical solutes with radii 0.6 and 1.2 nm in pure water and in 1 and 2 M NaCl solutions. The arrow indicates increasing salt concentration. (b) μ^{ex}/A for spherical solutes as a function of NaCl concentration in the solution. Density fluctuations, $p_{\nu}(N)$, for a spherical cavity of radius 1.2 nm sphere in (c) pure water and in (d) 1 M and (e) 2 M salt solutions: data from INDUS (symbols), Gaussian expectation (dashed blue line) and fits to theoretical prediction using eq 3 (solid red line).

ambient conditions.⁴¹ Whether the PMF is wholly convex or nonconvex has implications on the applicability of more efficient sparse sampling methods⁶⁷ to calculate free energies of dewetting of regions of interest in solution or near proteins.⁶⁸ Exploring these directions systematically would be an excellent direction to pursue in the future.

We also presented data from extensive simulations of the crossover in hydrophobic hydration focusing on the thermodynamics of crossover and salt effects on hydration. We studied shape dependence of hydrophobic hydration and showed that when the characteristic length remains small (comparable to the size of a water molecule), the nature of hydration of that object remains similar to small hydrophobes. This has implications on studies of hydrophobicity of surfaces with complex topography or in confinements. 70,71 We connect these observations to the nature of underlying density fluctuations in water, which confirms and adds to our understanding of lengthscale dependent hydrophobicity.

AUTHOR INFORMATION

Corresponding Author

Shekhar Garde — Howard P. Isermann Department of Chemical and Biological Engineering and Center for Biotechnology and Interdisciplinary Studies, Rensselaer Polytechnic Institute, Troy, New York 12180, United States; orcid.org/0000-0002-3307-6007; Email: gardes@rpi.edu

Authors

 Imee Sinha – Howard P. Isermann Department of Chemical and Biological Engineering and Center for Biotechnology and Interdisciplinary Studies, Rensselaer Polytechnic Institute, Troy, New York 12180, United States

Steven M. Cramer — Howard P. Isermann Department of Chemical and Biological Engineering and Center for Biotechnology and Interdisciplinary Studies, Rensselaer Polytechnic Institute, Troy, New York 12180, United States; orcid.org/0000-0003-4993-0826

Henry S. Ashbaugh — Department of Chemical and Biomolecular Engineering, Tulane University, New Orleans, Louisiana 70123, United States; o orcid.org/0000-0001-9869-1900

Complete contact information is available at: https://pubs.acs.org/10.1021/acs.jpcb.2c04990

Notes

The authors declare no competing financial interest.

ACKNOWLEDGMENTS

We express thanks for numerous insightful discussions with Dr. Amish Patel. S.G. and S.M.C. thank the NSF for Grant CBET-1704745 for partial financial support of this work. H.S.A. would like to thank the NSF for Grant CBET-1805167. We thank the Center for Computational Innovations at Rensselaer for their generous support of computational resources. It is a pleasure to contribute this manuscript to Pablo Debenedetti's Festschrift honoring his accomplishments. Pablo's research has greatly influenced our work in the area of water and hydration phenomena.

REFERENCES

- (1) Dill, K. A.; MacCallum, J. L. The protein-folding problem 50 years on. *Science* **2012**, 338, 1042–1046.
- (2) Tanford, C. Contribution of hydrophobic interactions to the stability of the globular conformation of proteins. *J. Am. Chem. Soc.* **1962**, *84*, 4240–4247.
- (3) Ball, P. Water as an active constituent in cell biology. *Chem. Rev.* **2008**, *108*, 74–108.
- (4) Privalov, P.; Khechinashvili, N. A thermodynamic approach to the problem of stabilization of globular protein structure: a calorimetric study. *J. Mol. Biol.* **1974**, *86*, 665–684.
- (5) Privalov, P. L. Stability of proteins small globular proteins. *Adv. Protein Chem.* **1979**, 33, 167–241.
- (6) Privalov, P. L.; Gill, S. J. Stability of protein structure and hydrophobic interaction. *Adv. Protein Chem.* **1988**, 39, 191–234.
- (7) Makhatadze, G. I.; Privalov, P. L. Contribution of hydration to protein folding thermodynamics: I. The enthalpy of hydration. *J. Mol. Biol.* **1993**, 232, 639–659.
- (8) Li, I. T.; Walker, G. C. Signature of hydrophobic hydration in a single polymer. *Proc. Natl. Acad. Sci. U. S. A.* **2011**, *108*, 16527–16532.
- (9) Ben-Amotz, D. Water-mediated hydrophobic interactions. *Annu. Rev. Phys. Chem.* **2016**, *67*, *617*–*638*.
- (10) Böhm, F.; Schwaab, G.; Havenith, M. Mapping hydration water around alcohol chains by THz calorimetry. *Angew. Chem., Int. Ed.* **2017**, *56*, 9981–9985.
- (11) Lee, J. Y.; Song, Y.; Wessels, M. G.; Jayaraman, A.; Wooley, K. L.; Pochan, D. J. Hierarchical Self-Assembly of Poly (d-glucose carbonate) Amphiphilic Block Copolymers in Mixed Solvents. *Macromolecules* **2020**, *53*, 8581–8591.
- (12) Jamadagni, S. N.; Godawat, R.; Garde, S. Hydrophobicity of proteins and interfaces: Insights from density fluctuations. *Annu. Rev. Chem. Biomol. Eng.* **2011**, *2*, 147–171.
- (13) Monroe, J.; Barry, M.; DeStefano, A.; Aydogan Gokturk, P.; Jiao, S.; Robinson-Brown, D.; Webber, T.; Crumlin, E. J.; Han, S.; Shell, M. S. Water structure and properties at hydrophilic and hydrophobic surfaces. *Annu. Rev. Chem. Biomol. Eng.* **2020**, *11*, 523–557.
- (14) Chandler, D. Interfaces and the driving force of hydrophobic assembly. *Nature* **2005**, *437*, 640–647.
- (15) Rajamani, S.; Truskett, T. M.; Garde, S. Hydrophobic hydration from small to large lengthscales: Understanding and manipulating the crossover. *Proc. Natl. Acad. Sci. U. S. A.* **2005**, 102, 9475–9480.

- (16) Pratt, L. R.; Pohorille, A. Theory of hydrophobicity: transient cavities in molecular liquids. *Proc. Natl. Acad. Sci. U. S. A.* **1992**, *89*, 2995–2999.
- (17) Hummer, G.; Garde, S.; Garcia, A.; Paulaitis, M. E.; Pratt, L. R. Hydrophobic effects on a molecular scale. *J. Phys. Chem. B* **1998**, *102*, 10469–10482.
- (18) Hummer, G.; Garde, S.; Garcia, A.; Pratt, L. New perspectives on hydrophobic effects. *Chem. Phys.* **2000**, 258, 349–370.
- (19) Stillinger, F. H. The Physical Chemistry of Aqueous System; Springer: 1973; pp 43–60.
- (20) Huang, D. M.; Geissler, P. L.; Chandler, D. Scaling of hydrophobic solvation free energies. *J. Phys. Chem. B* **2001**, *105*, 6704–6709.
- (21) Hummer, G.; Garde, S.; Garcia, A. E.; Pohorille, A.; Pratt, L. R. An information theory model of hydrophobic interactions. *Proc. Natl. Acad. Sci. U. S. A.* **1996**, 93, 8951–8955.
- (22) Godawat, R.; Jamadagni, S. N.; Garde, S. Characterizing hydrophobicity of interfaces by using cavity formation, solute binding, and water correlations. *Proc. Natl. Acad. Sci. U. S. A.* **2009**, *106*, 15119–15124.
- (23) Patel, A. J.; Varilly, P.; Chandler, D. Fluctuations of water near extended hydrophobic and hydrophilic surfaces. *J. Phys. Chem. B* **2010**, *114*, 1632–1637.
- (24) Beck, T. L.; Paulaitis, M. E.; Pratt, L. R. The potential distribution theorem and models of molecular solutions; Cambridge University Press: 2006.
- (25) Ashbaugh, H. S.; Vats, M.; Garde, S. Bridging Gaussian Density Fluctuations from Microscopic to Macroscopic Volumes: Applications to Non-Polar Solute Hydration Thermodynamics. *J. Phys. Chem. B* **2021**. *125*. 8152–8164.
- (26) Tanford, C. The hydrophobic effect: formation of micelles and biological membranes, 2nd ed.; J. Wiley: 1980.
- (27) Sarupria, S.; Garde, S. Quantifying water density fluctuations and compressibility of hydration shells of hydrophobic solutes and proteins. *Phys. Rev. Lett.* **2009**, *103*, 037803.
- (28) Rego, N. B.; Patel, A. J. Understanding hydrophobic effects: Insights from water density fluctuations. *Annu. Rev. Condens. Matter Phys.* **2022**, *13*, 303–324.
- (29) Patel, A. J.; Varilly, P.; Chandler, D.; Garde, S. Quantifying density fluctuations in volumes of all shapes and sizes using indirect umbrella sampling. *J. Stat. Phys.* **2011**, *145*, 265–275.
- (30) Berendsen, H.; Grigera, J.; Straatsma, T. The missing term in effective pair potentials. *J. Phys. Chem.* **1987**, *91*, 6269–6271.
- (31) Van Der Spoel, D.; Lindahl, E.; Hess, B.; Groenhof, G.; Mark, A. E.; Berendsen, H. J. GROMACS: fast, flexible, and free. *J. Comput. Chem.* **2005**, 26, 1701–1718.
- (32) Evans, D. J.; Holian, B. L. The nose-hoover thermostat. *J. Chem. Phys.* **1985**, *83*, 4069–4074.
- (33) Nosé, S. A unified formulation of the constant temperature molecular dynamics methods. *J. Chem. Phys.* **1984**, *81*, 511–519.
- (34) Hoover, W. G. Canonical dynamics: Equilibrium phase-space distributions. *Phys. Rev. A* 1985, 31, 1695.
- (35) Parrinello, M.; Rahman, A. Polymorphic transitions in single crystals: A new molecular dynamics method. *J. Appl. Phys.* **1981**, *52*, 7182–7190.
- (36) Darden, T.; York, D.; Pedersen, L. Particle mesh Ewald: An N log (N) method for Ewald sums in large systems. *J. Chem. Phys.* **1993**, 98, 10089–10092.
- (37) Humphrey, W.; Dalke, A.; Schulten, K. VMD: visual molecular dynamics. *J. Mol. Graphics* **1996**, *14*, 33–38.
- (38) Smith, D. E.; Dang, L. X. Computer simulations of NaCl association in polarizable water. *J. Chem. Phys.* **1994**, *100*, 3757–3766.
- (39) Huang, D. M.; Chandler, D. Cavity formation and the drying transition in the Lennard-Jones fluid. *Phys. Rev. E* **2000**, *61*, 1501.
- (40) Patel, A. J.; Varilly, P.; Jamadagni, S. N.; Hagan, M. F.; Chandler, D.; Garde, S. Sitting at the edge: How biomolecules use hydrophobicity to tune their interactions and function. *J. Phys. Chem. B* **2012**, *116*, 2498–2503.

- (41) Xi, E.; Marks, S. M.; Fialoke, S.; Patel, A. J. Sparse sampling of water density fluctuations near liquid-vapor coexistence. *Mol. Simul.* **2018**, *44*, 1124–1135.
- (42) Mittal, J.; Hummer, G. Static and dynamic correlations in water at hydrophobic interfaces. *Proc. Natl. Acad. Sci. U. S. A.* **2008**, *105*, 20130–20135.
- (43) Willard, A. P.; Chandler, D. Instantaneous liquid interfaces. J. Phys. Chem. B 2010, 114, 1954–1958.
- (44) Ashbaugh, H. S.; Truskett, T. M.; Debenedetti, P. G. A simple molecular thermodynamic theory of hydrophobic hydration. *J. Chem. Phys.* **2002**, *116*, 2907–2921.
- (45) Ashbaugh, H. S.; Pratt, L. R. Colloquium: Scaled particle theory and the length scales of hydrophobicity. *Rev. Mod. Phys.* **2006**, *78*, 159.
- (46) Sedlmeier, F.; Netz, R. R. The spontaneous curvature of the water-hydrophobe interface. *J. Chem. Phys.* **2012**, *137*, 135102.
- (47) Vega, C.; De Miguel, E. Surface tension of the most popular models of water by using the test-area simulation method. *J. Chem. Phys.* **2007**, *126*, 154707.
- (48) Garde, S. Sticky when dry. Nat. Chem. 2020, 12, 587-588.
- (49) Barnett, J.; Sullivan, M. R.; Long, J. A.; Tang, D.; Nguyen, T.; Ben-Amotz, D.; Gibb, B. C.; Ashbaugh, H. S. Spontaneous drying of non-polar deep-cavity cavitand pockets in aqueous solution. *Nat. Chem.* **2020**, *12*, 589–594.
- (50) Athawale, M. V.; Goel, G.; Ghosh, T.; Truskett, T. M.; Garde, S. Effects of lengthscales and attractions on the collapse of hydrophobic polymers in water. *Proc. Natl. Acad. Sci. U. S. A.* **2007**, 104, 733–738.
- (51) van der Vegt, N. F. Length-scale effects in hydrophobic polymer collapse transitions. J. Phys. Chem. B 2021, 125, 5191–5199.
- (52) Hummer, G.; Garde, S. Cavity expulsion and weak dewetting of hydrophobic solutes in water. *Phys. Rev. Lett.* **1998**, *80*, 4193.
- (53) Huang, D. M.; Chandler, D. Temperature and length scale dependence of hydrophobic effects and their possible implications for protein folding. *Proc. Natl. Acad. Sci. U. S. A.* **2000**, *97*, 8324–8327.
- (54) Ashbaugh, H. S. Entropy crossover from molecular to macroscopic cavity hydration. *Chem. Phys. Lett.* **2009**, 477, 109–111.
- (55) Garde, S.; Hummer, G.; García, A. E.; Paulaitis, M. E.; Pratt, L. R. Origin of entropy convergence in hydrophobic hydration and protein folding. *Phys. Rev. Lett.* **1996**, *77*, 4966.
- (56) Patel, A. J.; Varilly, P.; Jamadagni, S. N.; Acharya, H.; Garde, S.; Chandler, D. Extended surfaces modulate hydrophobic interactions of neighboring solutes. *Proc. Natl. Acad. Sci. U. S. A.* **2011**, *108*, 17678–17683.
- (57) Baldwin, R. L. How Hofmeister ion interactions affect protein stability. *Biophys. J.* **1996**, *71*, 2056–2063.
- (58) Collins, K. D. Charge density-dependent strength of hydration and biological structure. *Biophys. J.* **1997**, *72*, 65–76.
- (59) Zhang, Y.; Cremer, P. S. Interactions between macromolecules and ions: the Hofmeister series. *Curr. Opin. Chem. Biol.* **2006**, *10*, 658–663.
- (60) Thosar, A. U.; Patel, A. J. Hydration determines anion accumulation. *Nat. Chem.* **2022**, *14*, 8–10.
- (61) Kalra, A.; Tugcu, N.; Cramer, S. M.; Garde, S. Salting-in and salting-out of hydrophobic solutes in aqueous salt solutions. *J. Phys. Chem. B* **2001**, *105*, 6380–6386.
- (62) Athawale, M. V.; Sarupria, S.; Garde, S. Enthalpy- entropy contributions to salt and osmolyte effects on molecular-scale hydrophobic hydration and interactions. *J. Phys. Chem. B* **2008**, *112*, 5661–5670.
- (63) Ben-Amotz, D. Global thermodynamics of hydrophobic cavitation, dewetting, and hydration. *J. Chem. Phys.* **2005**, *123*, 184504.
- (64) Ben-Amotz, D.; Omelyan, I. P. The influence of molecular shape on chemical reaction thermodynamics. *J. Chem. Phys.* **2001**, 115, 9401–9409.
- (65) Stamatopoulou, A.; Ben-Amotz, D. Cavity formation free energies for rigid chains in hard sphere fluids. *J. Chem. Phys.* **1998**, 108, 7294–7300.

- (66) Reiss, H. Scaled particle methods in the statistical thermodynamics of fluids. Adv. Chem. Phys. 1965, 9, 1–84.
- (67) Patel, A. J.; Garde, S. Efficient method to characterize the context-dependent hydrophobicity of proteins. *J. Phys. Chem. B* **2014**, *118*, 1564–1573.
- (68) Xi, E.; Remsing, R. C.; Patel, A. J. Sparse sampling of water density fluctuations in interfacial environments. *J. Chem. Theory Comput.* **2016**, *12*, 706–713.
- (69) Giovambattista, N.; Debenedetti, P. G.; Rossky, P. J. Hydration behavior under confinement by nanoscale surfaces with patterned hydrophobicity and hydrophilicity. *J. Phys. Chem. C* **2007**, *111*, 1323–1332.
- (70) Ferguson, A. L.; Giovambattista, N.; Rossky, P. J.; Panagiotopoulos, A. Z.; Debenedetti, P. G. A computational investigation of the phase behavior and capillary sublimation of water confined between nanoscale hydrophobic plates. *J. Chem. Phys.* **2012**, *137*, 144501.
- (71) Sharma, S.; Debenedetti, P. G. Free energy barriers to evaporation of water in hydrophobic confinement. *J. Phys. Chem. B* **2012**, *116*, 13282–13289.

□ Recommended by ACS

Molecular Structure and Dynamics in Wet Gecko β-Keratin

Hossein Eslami, Florian Müller-Plathe, et al.

DECEMBER 16, 2022

ACS BIOMATERIALS SCIENCE & ENGINEERING

RFAD 🗹

Size-Dependent Order-Disorder Crossover in Hydrophobic Hydration: Comparison between Spherical Solutes and Linear Alcohols

Vrushali Hande and Suman Chakrabarty

JANUARY 12, 2022

ACS OMEGA

READ 🗹

Local Ice-like Structure at the Liquid Water Surface

Nathan L. Odendahl and Phillip L. Geissler

JUNE 13, 2022

JOURNAL OF THE AMERICAN CHEMICAL SOCIETY

READ 🗹

Solubility Prediction of Organic Molecules with Molecular Dynamics Simulations

Zoran Bjelobrk, Marco Mazzotti, et al.

JULY 29, 2021

CRYSTAL GROWTH & DESIGN

READ 🗹

Get More Suggestions >